Research & Reviews: Journal of Material Sciences e-ISSN: 2321-6212

Nanoindentation to Microhardness to Tensile Strength Correlation Coefficient Estimates in Relation to Microstructure in Eutectic Snbi Alloy

Nataliya Starostina*

Department of Mechanical Engineering, Santa Clara University, California, USA

Research Article

Received: 23-Aug-2024, Manuscript No. JOMS-24-143130; **Editor assigned:** 26-Aug-2024, PreQC No. JOMS-24-143130 (PQ); **Reviewed:** 09-Sep-2024, QC No. JOMS-24-143130; **Revised:** 16-Sep-2024, Manuscript No. JOMS-24-143130 (R); **Published:** 23-Sep-2024, DOI: 10.4172/2321-6212.12.3.001

***For Correspondence:**
Nataliya Starostina, Department of Mechanical Engineering, Santa Clara University, California, USA

E-mail:
nataliya.starostina@gmail.com

Citation: Nataliya S. Nanoindentation to Microhardness to Tensile Strength Correlation Coefficient Estimates in Relation to Microstructure in Eutectic Snbi Alloy. RRJ Mater Sci. 2024;12:001.

ABSTRACT

Determining strength to hardness correlation coefficients on nano and microscale in correspondence to microstructure and composition leads the way to inexpensive, non-destructive ways to predict tensile strength of bulk materials which is important for developing preventive maintenance procedures in the variety of industries. Nanohardness and microhardness tests were performed on an in-house prepared eutectic SnBi alloy. Elemental composition and eutectic morphology were verified by scanning electron microscopy and energy dispersive spectroscopy. Linear correlation coefficients, C_1, between nanoindentation and Vickers microhardness, was determined based on experimental measurements and found to be greater than 1.25. Tabor factor, the ratio of Vickers microhardness to ultimate tensile strength, was estimated to be consistently greater than 3. Comparison to coefficients estimated from data available for other alloy systems is discussed.

Keywords: SnBi alloy; Tabor factor; Nanoindentation hardness to Vickers hardness coefficient; Eutectic microstructure; Nano-micro-hardness to tensile strength correlation; Non-destructive testing

INTRODUCTION

The most compelling points of importance correlating Nano Indentation (NI) hardness measurements to Ultimate Tensile Strength (σUTS) are outlined by brooks and walley [1-2]. First, reliable hardness-strength correlation facilitates fast and inexpensive mechanical properties evaluation. Second, non-destructive tests, such as hardness measurements, allow inspection of in-service and in-service conditions without harming the equipment [3].

The third important point is that very little quantity of materials is required for hardness testing as opposed to American Society for Testing and Materials (ASTM) tensile tests. Rapid developments of synthetic methods of fabrication necessitate a pivot to more localized testing techniques [4-10], such as microhardness and NI.

A well-known Hall-Petch relationship, that is the grain size dependence of yield strength of metallic materials, was established in early 1950 for pure metals, critically reviewed over last six decades and adopted by reputable textbooks in materials science [11-15]. However, it relates yield strength, not tensile strength, to microstructure or grain size for a given alloy. Therefore, considerations for grain size and composition are among the most important factors to affect strength of materials [16,17]. Tabor correlated hardness to tensile strength, k=H/σUTS, by a factor of ~3 in 1951. In 1972, Cahoon refined the relationship suggesting σUTS to be between H/2.9 and H/3.1. There were no assumptions made regarding microstructure or composition in those papers [18,19]. The most widely used empirical relations of tensile strength to Vickers Hardness (HV),

$$HV \approx 3\sigma UTS \text{ or } k=Hv/\sigma UTS \approx 3, \text{ where k is Tabor factor} \quad (1)$$

is established for carbonized and alloyed steels after different heat treatments. Notably, the same proportionality relationship does not hold for all metals and alloy in relation to Brinell hardness, HB. A distilled relation specifically for steels was adopted in textbooks HB=3.45σUTS. Callister points out the difference in the coefficient between steel, nodular cast iron and brass. Therefore, it should not be expected k=3 ratio to hold for Vickers hardness for all metals and alloys. The importance of tying the Tabor factor to the grain size and crystallography of the material is indicated in reviews by Kumar, Broitmen and later by Pintaude [20-22]. Excellent overviews of developments in hardness measurements in recent years and over last six decades are available in literature. K=3 relationship has been proven for coarse-grained polycrystalline materials, specifically carbon and alloy steels after annealing, normalization and quench-to-temper conditions. Both experiments and the general theory of the relationship between microscopic hardness and macroscopic strength with reference to microstructure, composition, heat and mechanical treatment are described in literature [1,16,17,21-24]. The reported range of linear coefficient, k, referring to Vickers hardness, is 2.8-3.36 [1,17,23,25]. The main categories for Tabor factor are related to material's microstructure and ability to deform plastically are

a) k~3, micro size grains, mixed failure (2)

b) k>3, micro and nanostructure, cold work, severe deformation, brittle failure (3)

c) k<3, ultrafine grains, annealed, ductile failure (4)

Tabor factor is reportedly linked to the grain size, crystallinity, presence of the second phase (s), number of phases, chemistry of bonding and heat/mechanical treatment. Strong deviation from relation (2) or 4<k<8 is reported for brittle nanocrystalline materials, relation (3). Khodabakhshi's group is focused on fine grained and ultrafine grained metals and alloys reinforced by secondary phase and processed by severe plastic deformation (friction stir process) [17,23]. Their group reveals that hardness-strength relations do not obey the established relationship for coarse-grained materials, relation [1]. Khodabakhshi's group reports the inability to offer a general linear correlation between microhardness and tensile strength for metal matrix nanocomposites due to structural heterogeneity [23]. Analysis of the microhardness-tensile strength relationship for nanofabricated crystalline materials is reported in the literature, considering the effect of heat treatment and cold work without specifying grain size [1,21-25].

Furthermore, on nanoscale, there is also a linear relationship between NI hardness, Health Information Technology (HIT) and Vickers microhardness,

$$HIT=C1\ HV \text{ or } C1=HIT/HV \quad (5)$$

where C1 is a linear coefficient between nanoindentation and microhardness [26-28]. The reasons why C1 is not equal 1.0 or why "HIT" is not the same as "HV" are discussed in literature [27,28]. Different values (C1>1) are reported for single crystals and polycrystalline metals and alloys [27-29]. No correlation is found for rubbers and diamond-like carbon films [27]. The reported values for C1 could be categorized as following.

a) C1>1.13 for single crystals (6)

b) C1>1.25 for polycrystalline metals and alloys (7)

Elastic anisotropy, polycrystallinity, imperfections, morphology of microstructure, chemical composition, mechanical and heat treatment [26-32] can influence the actual value of C1, relation 5. Geng's theoretical model connecting micro and nanohardness supported by experimental data performed on Fe-Cr alloys, without specifying the microstructure of the alloy under study, concludes that quantitative corrections for pileups are similar in nano and micro-scale measurements [30]. Geng's suggests the possibility of a universal linear relationship for all metallic materials, σUTS ~ HIT. Assuming a vast amount of experimental data supports numerical values for the correlation coefficients, C1 and k, the relationship σUTS=HIT /C1k, could be of value for practical reasons. It enables a forecast of tensile strength based on nanohardness.

Our goal in this paper is to determine coefficient, C1 and estimate Tabor factor, k, for eutectic SnBi alloy in correspondence to microstructure and composition without any additional mechanical or heat treatment. We intend to pioneer consistent study by starting with a polycrystalline substitutional binary alloy having eutectic microstructure after slow solidification. So far, we could not find systematic studies on hardness-strength correlation considering all variables listed above. Our second goal is to verify the reported finding by Xiaowu's group allowing to estimate Vickers hardness based on eutectic morphology measurements [33]. Obtaining hardness from interlamellar distance measurement directly could be of technological importance because microhardness test is skipped. Our third goal is to verify consistency of experimental results in comparison to the calculated coefficients based on data available in literature [25,27,30,34-42]. The choice of the material is driven by a quest of the microelectronic industry for lead-free solder to replace primarily used solder materials such as SnPb due to detrimental effects on human health and environment contamination [42-46]. SnBi alloy, with its similarity to SnPb in phase transformations, has been a promising candidate because of its low melting point (138.8°C) [42]. Tin-bismuth solder has been extensively investigated in terms of composition, morphology, strength, hardness and creep behavior [33-40].

MATERIALS AND METHODS

Raw materials and sample preparation

SnBi alloy of 58 wt%Bi was prepared at the Santa Clara University materials laboratory. Chemically pure, 99.9%, Sn and Bi were purchased from Sigma-Aldrich and Fisher Chemical, respectively. The powders of the desired proportion were weighed, manually mixed, stirred, then melted and solidified twice before preparation for microstructure observations. 10 grams' total weight of alloy was prepared, with an accuracy of better than 0.1 grams, so that would correspond to an error of less than 1 wt%. A thermocouple was immersed into the melt to monitor the cooling rate overnight in the air. A slight compositional gradient and variation in microstructure was expected due to variations in the cooling rate. 4 Two disc-shape samples 1 cm diameter 2-3 mm tall were embedded in epoxy mount for mechanical polishing and handling. Specimens were ground with 240, 400 and 600 grit SiC papers (Buehler), followed by polishing with 1.0-, 0.3 and 0.05-micron alumina powder suspended in water. The epoxy mount was later removed before characterization with Scanning Electron Microscope (SEM) to avoid surface charging issues.

Materials characterization methods and image analysis

4 Two disc-shape samples 1 cm diameter 2-3 mm tall were embedded in epoxy mount for mechanical polishing and handling. Specimens were ground with 240, 400 and 600 grit SiC papers (Buehler), followed by polishing with 1.0-, 0.3 and 0.05-micron alumina powder suspended in water. The epoxy mount was later removed before characterization with Scanning Electron Microscope (SEM) to avoid surface charging issues. 2.2 Materials characterization methods and image analysis. The microstructural morphology of the SnBi sample was done by SEM, using a Hitachi S-4800. Elemental mapping and composition verification was done by Energy Dispersive Spectroscopy (EDS), using X-Max detector oxford Instruments. Backscattered Electrons (BSE) were used for atomic composition contrast imaging. BSE images were transferred to an EDS detector equipped with AZtec software for elemental mapping and compositional analysis. Two different areas of the sample were examined at different magnifications. Ten BSE images and four EDS maps were acquired for analysis. MATLAB and ImageJ software were used for image analysis based on atomic contrast. Colony boundaries were marked with white lines. 9 colonies, 66 aspect ratios and 98 interlamellar distances were measured altogether. Microhardness was evaluated by the Vickers method using a leco LM 248AT test machine with an applied load of 1N. The leco LM 248AT test machine was equipped with a 4-side pyramidal diamond indenter and Cornerstone software allowing semi-automated HV measurements from digital display. The microhardness test was repeated for 8 trials on the same sample. The tests were performed randomly on the sample without attempting to decern effect of different phases. Vickers indentations were done with each indentation being two sizes of the indent area apart from each other in both directions to avoid influence of adjacent indentations. A hysitron TI Premier nanoindenter, equipped with a berkovich tip, was used for nanoscale hardness measurements in static mode [47,48]. Nanoindentations were done on the samples in a 2 x 2 array, with each indentation 50 μm apart in both directions to avoid influence of adjacent indentations. A peak load of 5,000 μN was used. 2400 data points per load/unload curve were acquired. The tests were performed randomly on the sample without attempting to decern effect of different phases. A Hysitron TI nanoindenter is equipped with a software package which outputs the standard NI parameters for each acquired load/unload curve.

RESULTS

Elemental composition verification based on EDS

Shown in Figure 1A is a representative EDS map, with green corresponding to Bi and red to Sn. Aztec software estimates 55 wt%Bi as a total composition. An x-ray spectrum collected from the entire image is shown in Figure 1B.

There was no evidence of impurities present in the alloy. Overall, EDS measurements for the entire sample indicated composition variation in the range of 5 wt%Bi, resulting to 55 ± 2.5 wt%Bi. Elemental composition results along with SnBi phase diagram are shown in Figure 2.

However, AZtec measures the ratio of the longest side to the shortest, which is reciprocal from what ImageJ measures-the shortest side to the longest.

The reciprocal of the measured EDS AZtec ratio comparable to the BSE ImageJ range is then found to be 0.47-0.5. The irregular shape of individual lamellas is consistent between BSE and EDS images.

Figure 1. (A) Representative EDS map collected from the entire area. Red corresponds to the Sn-rich phase and green to the Bi-rich phase. (B) An X-ray spectrum collected from the area with corresponding total composition 55 wt%Bi and 45 wt%Sn. **Note:** (■) Sn-rich phase; (■) Bi-rich phase.

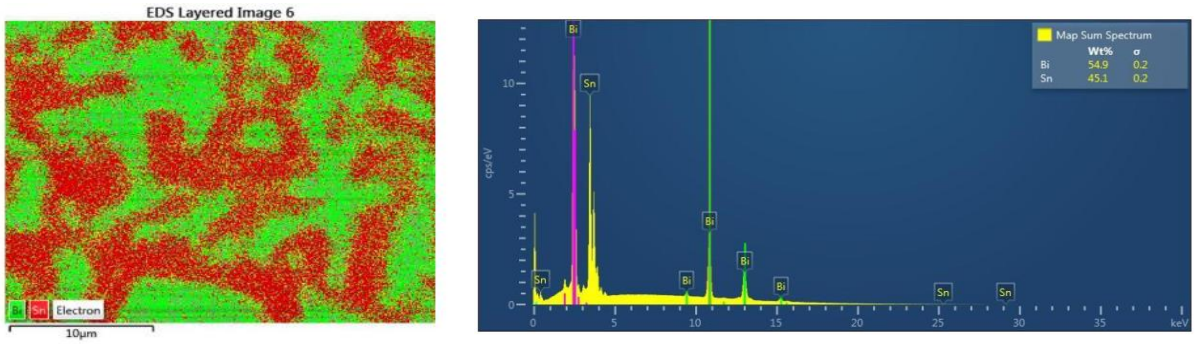

(A) (B)

Figure 2. (A) NIST calculated SnBi phase diagram indicating eutectic composition for SnBi alloy, 57.97 wt%Bi. (B) The composition of in-house SnBi alloy based on EDS data (blue) is 55 ± 3 wt%Bi. Eutectic 6 composition, 58 wt%Bi, is shown in black. Compositions of alloys our results being compared to are shown in yellow, 50 wt%Bi and orange, 58 wt%Bi, respectively [42].

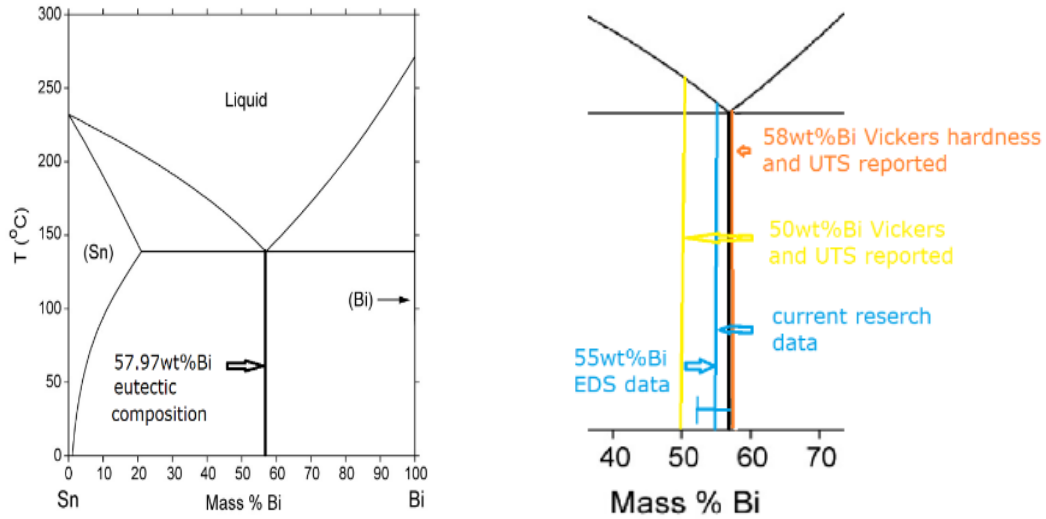

(A) (B)

Microstructure, eutectic morphology characterization based on atomic contrast

BSE images from a difference in atomic numbers of constituent elements can be seen for the SnBi alloy in Figure 3. The outlines of colonies for size measurements are drawn in ImageJ [49-51]. The average colony size ranged from 1,608 to 1,211 µm^2. This leads to the average colony size being in the range of 35-40 µm, assuming a square root relationship between area and size.

Figure 3. SEM images of different areas of the same sample.

Four colonies were measured in the image shown. Magnification is 1,300 x (A) and five colonies in the image shown of 7 the same sample. Magnification is 1,000 x (B). The average of these two colony sizes is 1,608 ± 336 μm^2, size of ~40 µm (A) and 1,211 ± 354 μm^2, size of ~35 µm (B), respectively. **Note:** Slightly different magnification of two images. Brighter areas are Bi-rich, while darker areas indicate Sn-rich phases. The direction of polishing marks, scratches and contamination particles can be observed. Colony boundaries are marked with white lines.

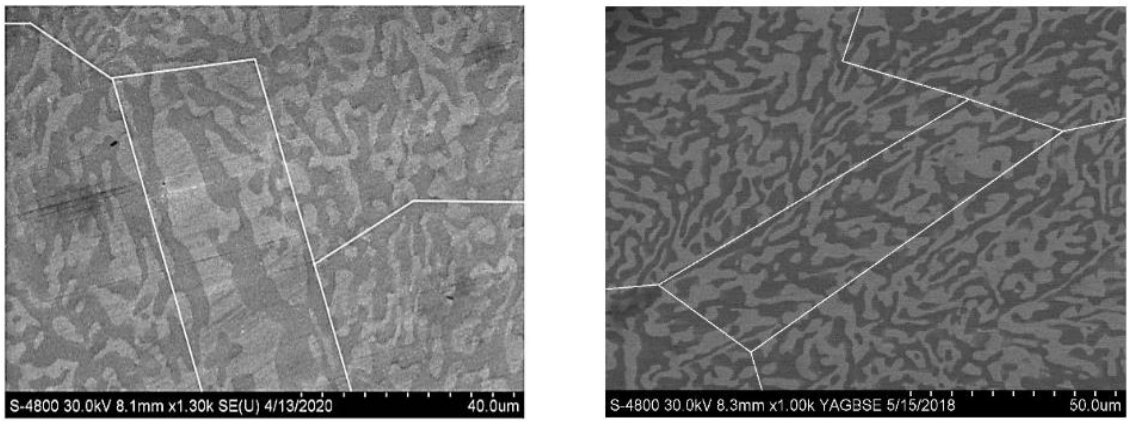

(A) (B)

The mean aspect ratio of the Bi-rich phase was found to be 0.42 and 0.83, depending on the size of the colony, with larger islands having larger aspect ratios, Figure 4.

Figure 4. MATLAB hand-drawn aspect ratios for smaller. **Note:** (A) Bismuth islands with 40 measurements in the image shown and larger; (B) Bismuth islands with 26 measurements for the same BSE image shown. The mean aspect ratio was found to be 0.42 (A) and 0.83 (B).

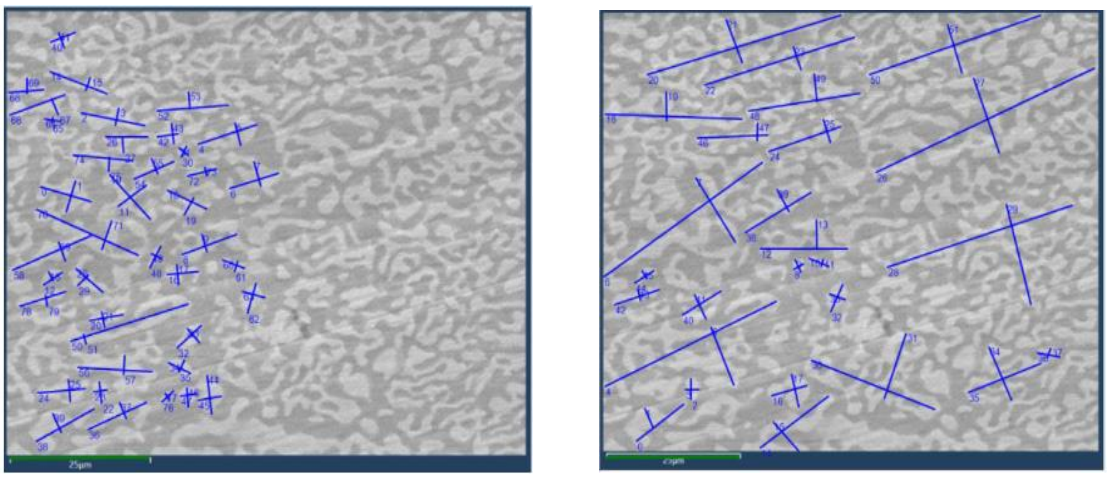

(A) (B)

The interlamellar spacing between the two phases ranges between 7.2 ± 1.9 µm for one area, Figure 5-A and 4.5 ± 0.8 µm for another area on the same sample, Figure. 5B. The measured interlamellar distance on average is ~6 µm. The interlamellar spacing as the distance between the centers of two adjacent lamellas [14,52]. If the average colony size is about 35-40 microns with interlamellar distance of 6 microns, we can reasonably assume that the size of individual lamellas is about ~ 6-7 µm. The observed morphology of individual lamellae was found to be of an irregular shape and consistent with EDS observations.

Figure 5. Interlamellar distance measurements are shown for two different areas of the same sample. BSE images were taken at different magnification. An average of 28 measurements in the BSE image shown found interlamellar distance to be 7.2 ± 1.9 μm for area. Magnification 2,000 x (A) and an average of 98 measurements in the BSE image shown averaged 4.5 ± 0.8 μm for area. Magnification 1,000 x (B), respectively.

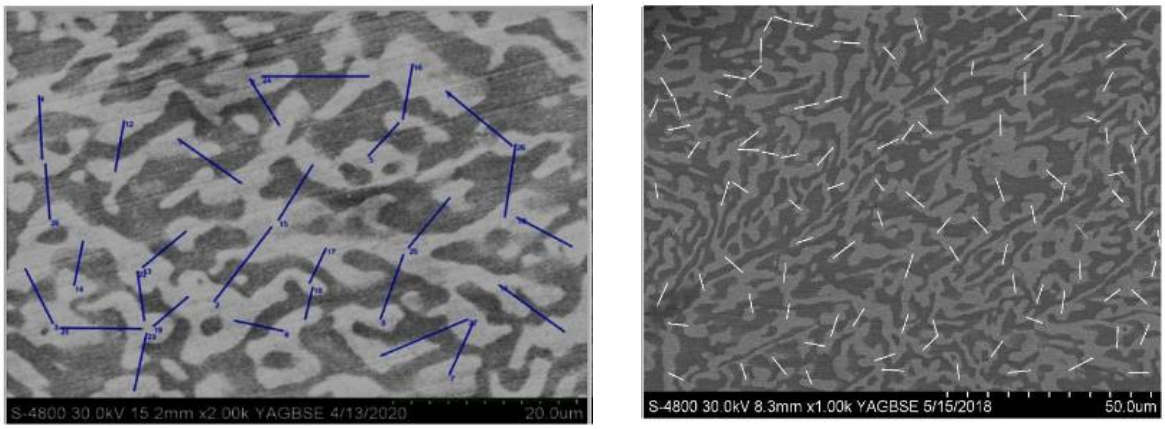

(A) (B)

The results of size and interlamellar distances are summarized in Table 1. The colony size is estimated as 35-40 um or fine-grained material. The interlamellar spacing between the two phases ranged from 7.2 ± 1.9 μm to 4.5 ± 0.8 μm for one area to another area on the same sample. The average size of individual lamellas is about 6 μm, corresponding to the low end of fine-grained microstructure.

Table 1. Eutectic morphology characteristics measured from BSE data, measured vickers hardness, estimated vickers hardness, measured and reported [34] NI hardness results summary.

Colony size, μm	Average interlamellar distance, μm	Hv, measured, Mpa	Hv, estimated based on measured interlamellar distance, MPa	HIT, measured, Mpa	HIT, reported [34] Mpa	C1=HIT/HV
35-40	6	193.5 ± 18.8	235 ± 35	340 ± 11	287	1.2-1.8

Vickers and nanoindentation measurements: Estimating linear correlation coefficients: k and C_1

Nanoindentation tests data and representative load/unload curve are shown in Table 2 and Figure 6. The average nanoindentation hardness, HIT, was measured to be 340 ± 11 MPa.

Table 2. Nanoindentation measurements data. Representative load/unload curve is shown on Figure 6.

Max load, μN	Max depth, nm	Stiffness (μN/nm)	Reduces modulus, GPa	Nano hardness, GPa
4975.0 ± 6.5	758.9 ± 12.3	251.7± 7.5	58.262 ± 0.9	0.340 ± 0.01

Figure 6. Representative nanoindentation test load/unload curve for eutectic SnBi alloy. The measurements data summarized in Table 2.

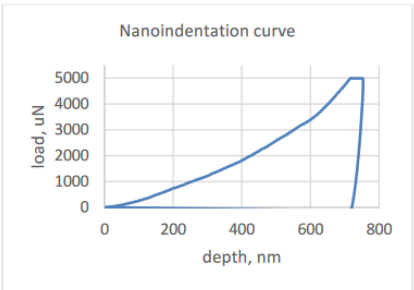

The average Vickers hardness, HV, was measured to be 193.5 ± 18.8 MPa. A correspondence between interlamellar spacing and Vickers hardness for 58 wt%Bi alloy [33] was reported as following: The spacing from 1.4-10 μm corresponds to 27-20 HV (kg/mm^2) or 200-270 MPa. Expected hardness and measured hardness, 193.5 ± 18.8 MPa, being in good agreement with each other, are summarized along with morphology data in Table 2. The correlation coefficient, k, was calculated using Tabor factor definition (1). First, we estimated k for 55 wt%Bi alloy based on our values for Hv and reported σUTS data [37], Table 3. k is found to be in the range of 3.6-4.4, averaging ~4.0. For 58 wt%Bi alloy two values of hardness and two values of σUTS are reported. If the reported σUTS=63.6 MPa [37] and 60.2 MPa [45] is assumed for reported range of Hv, 200-287 MPa [33], then the Tabor factor is 3.1-4.8. If the reported σUTS=63.6 MPa [37] and 60.2 MPa [45] is assumed for reported hardness, Hv=210 [36], then the Tabor factor is 3.3-3.5, (Table 3). Evidently, the variation due to solidification rate (interlamellar distances) in reported Hv and σUTS for a given composition influences the results for a given composition and the type of microstructure. Nevertheless, Tabor factor is consistently being greater than 3, as shown in Table 3.

Table 3. Tabot factor, k, estimated for 55 wt%Bi, 58 wt%Bi, depending on measured and reported Hv and σUTS.
Note: *HV=193.5 (measured), **HV=235 (estimated based on measured interlamellar distance).

Composition, wt%	Bi HV, MPa	σUTS, MPa	Tabor factor, k
55	193.5*-235**	53.1 [37]	3.6-4.4
58	210 [36]	60.2 [45]	3.3-3.5
	200-287 [33]	63.6 [37]	3.1-4.8

DISCUSSION

Composition, microstructure in correspondence to nano and micro hardness

EDS analysis yielded 55 ± 2.5 wt%Bi in-house made alloy composition. EDS, phase diagram and original weight agree within a margin of error of electron microscopy and manual sample preparation. The morphology observations closely resemble the morphology of 58 wt%Bi alloy [44]. Our EDS data indicates no presence of second phase inclusions, as one may have been expected for off-eutectic composition. Therefore, we do not expect a significant variation in microstructure within ± 2.5 wt%Bi near eutectic. In-house made alloy has fine grained microstructure strengthened by eutectic lamellas with interlamellar distances of 6 μm, Table 1. BSE and Vickers hardness measurements confirm the reported ability to estimate Hv from interlamellar distances of the eutectic [33], Table 2. We anticipate it could be of technological importance to be able to predict Vickers hardness based on interlamellar spacing without performing vickers hardness tests.

Microstructural changes due to different rates of solidification of eutectic alloy differ in interlamellar spacing: Larger distances correspond to lower hardness and strength and smaller distances-to higher hardness and strength. The range of hardness's can be bracketed based on reported data for interlamellar distances and found to be between 200-287 MPa [33]. Since our BSE and EDS measurements show no presence of a second phase, only eutectic morphology, we find it justifiable to use reported σUTS from different sources to bracket variation of Tabor factor for eutectic and near eutectic composition, Table 3. Notably, NI hardness data reported by Shen's group for 50-70 wt% of Bi stay at about the same value [34]. σUTS reported data vary due to different rates of solidification and therefore slightly different microstructure. However, the microstructure remains eutectic, therefore it is reasonable to expect that mainly eutectic phase strengthening may affect C1 and Tabor factor.

Tabor factor, k-in correspondence to strengthening mechanisms

k>3 at and near eutectic composition leads us to believe we are observing the effect of strengthening by eutectic phase. In fact, strengthening by eutectic is the dominating strengthening mechanism present in our alloy. It is well known [16,17]. that alloys become harder, stronger if strengthened by a second phase or eutectic phase because additional obstacles provided to impede dislocations flow. Riba's data reporting microhardness, tensile strength and %elongation for SnBi alloy support that statement. Decrease in ductility, %elongation, or becoming more brittle is expected for eutectic alloys in comparison to pure components (Sn and Bi), solid solution strengthened (SnBi binary alloy, not eutectic SnBi alloy) and grain size strengthened alloy of the same composition. However additional experimentation is planned to provide experimental evidence for individual cases. If our assumption of strengthening by eutectic is valid it would bring Tabor factor to be >3 according to Zhang's classification [24]. which is in good agreement with our data.

Additional strengthening, strengthening by dislocation, may manifest itself as k>3, k=3.4 and k=3.5 was reported for cold rolled copper and Cu 35 wt%Zn alloy respectively. It appears the correlation was stronger for solid solution strengthened and work-hardened alloys, $k \approx 3$, relation (2) as opposed to annealed elemental metal and binary alloy, k<3, relation (3). k=2.4 for annealed copper and k=2.0, Cu 35 wt%Zn alloy were reported [24]. Tabor factor estimates for second phase strengthened alloys were also reported in literature. The experimental work done on steels resulted in 2.6<k<3.3 and 3.0<k<3.4, respectively [25,29]. Yakubtsov's group reports Vickers hardness and σUTS data for slow, mid and fast cooling rates [25]. Our data, 3.6<k<4.4, is in better agreement with data obtained on steels, second phase(s) reinforced material, rather than with elemental metal, Cu and substitutional CuZn alloys. The list of investigated materials in the Table 4 is organized as following: top row-single crystal elemental metal, second row–annealed polycrystalline metals, third-substitutional polycrystalline binary alloy, fourth and fifth-cold worked metal and alloy, middle rows-second phase strengthened alloys, nanocrystalline metals and composites subjected to severe plastic deformation listed on the bottom. It is notable that tabor factor is to increase as the number of strengthening mechanisms increases. Also, the suggested classification, relations (2,3,4), seem to work well for micro grained materials, while on nanoscale the results are inconsistent [24].

C1-in correspondence to the method of measurement, strengthening and σUTS forecast

The topic of correlation between NI and Vickers hardness from perspective of hardness measurement techniques was not directly discussed in the original oliver and parr paper [28]. Oliver and Pharr demonstrated that a 4-sided pyramidal vickers indenter has the same area function as a 3-sided Berkovich indenter [47,48]. The original paper also emphasizes that the procedure for determining the area function does not require imaging of indentation. Visualization of the indent is required in traditional methods (Vickers, Knoop, Brinell, Rockwell). The fundamental difference between NI and vickers hardness manifests itself in using projected area as opposed to measured total contact area of the imprint. This key difference results in a discrepancy between the hardness measurements obtained from each technique. The errors in depth-to-area conversions (pile-up/sink-in, even though effects are counterproductive; elastic anisotropy, etc.) represent a secondary source of hardness discrepancies, therefore, making C1 likely to be greater than 1.0. Nanoindentation size effect can be considered negligible because measured penetration depth is large, 758.9 ± 12.3, Table 2. Nanoindentation size effect is pronounced at shallow indentation depth according to the review paper [53].

For the SnBi alloy tested, the correlation coefficient was found to be 1.5 on average. Our results suggest a stronger correlation than forecasted by sawa [37] for both single crystals, C1=1.13 and polycrystals, C1=1.25, Table 4. Taylor's group [29] reported a significant amount of hardness *vs*. strength data for DP980 steel, estimating the range for the C1 coefficient to be between 1.5 and 2.0. Taylor's group results also indicated a stronger, C1>1.25, correlation between nanoindentation hardness and Vickers hardness [27], Table 4. Our results are in good agreement with Taylor's group. We attribute the stronger correlation, C1>1.25, to the presence of the second phase(s) in steels and eutectic phase in SnBi alloy. Assuming a vast amount of experimental data supports numerical values for the correlation coefficients, C1 and k, the relationship σUTS=HIT /C1k, may allow forecast tensile strength from nanoindentation measurements. The ability to predict macroscopic strength from nanohardness measurements can be very important from a technological point of view. This study is a first step toward that goal. Table 4. Hardness-strength linear correlation coefficients C1 and k estimated for different metals and alloys as a function of crystallinity, grain size, presence of second phase, mechanical and heat treatment. A value of *C1 and *k coefficients were calculated based on experimental data available from Taylor [29]. **k coefficient was calculated based on experimental data available from Yakubtsov [25].

C1=HIT/HV	Tabor factor k=HV/σUTS	Grain size, μm	Second phase	Material, composition and processing	Research groups
1.13	n/a	n/a	no	Single crystal Cu	Sawa [27]
n/a	2.44	n/a	no	Annealed Cu	Zhang et al. [24]
n/a	2.03	n/a	no	Annealed Cu32 wt%Zn	Zhang et al. [24]
n/a	3.41	n/a	no	Cold rolled Cu	Zhang et al. [24]
n/a	3.45	n/a	no	Cold rolled Cu32 wt%Zn	Zhang et al. [24]
1.25	n/a	n/a	yes	SK85 steel	Sawa [27]
1.2-1.8	3.6-4.4	35-40	yes	Sn55 wt%Bi	Present work
1.5-2.0*	3.0-3.4*	n/a	yes	DP980 steel	Taylor et al.[29]
n/a	2.64-3.33**	30-40	yes	Bainitic low carbon steel	Yakubtsov et al.[25]
n/a	~3.36 with significant scatter	0.2-1.4	-	AlMg alloy nanoparticles reinforced, friction stir processed	Khodabakhshi et al. 2020 [17]
n/a	<3	Ultra-fine grained	-	Al, AA 3003 Al alloy, Cu, Ni, Ti, low carbon steel; friction stir processed	Khodabakhshi et al.2015 [23]
n/a	~3.0	0.005	-	Electroformed nanocrystallines	Brooks et al.[1]

CONCLUSION

Our work pioneers systematic study bridging the gap between NI hardness and σUTS for 55 ± 2.5 wt% SnBi alloys. NI to vickers hardness linear correlation coefficient, C1, is found to be greater than 1.25. The Tabor factor, k, is found to be consistently greater than 3. The correlation stronger than for single crystals and substitutional binary alloys is observed. Our data suggest that strengthening by eutectic phase may influence the correlation. Our data are in good agreement with previously reported data for annealed fine-grained polycrystalline second-phase strengthened alloys without mechanical treatment. We would like to conclude that considering the microstructure, composition and strengthening mechanism for hardness-strength studies could be very important.

FUNDING

No funding was received for conducting this study and manuscript preparation.

ACKNOWLEDGMENT

We would like to acknowledge the contributions of Jamie Ferris, teaching assistant, for helping with mechanical measurements, Dr. M. McElfresh for review the manuscript, Dr. R. Marks for supplying samples and Prof. D. Fabris for support of the MECH333B laboratory course.

ETHICAL STANDARDS

There was no research involving Human Participants and/or animals. All authors conducted research and submitted original manuscript in compliance with ethical standards.

COMPETING INTERESTS

Dr. Nataliya Starostina, adjunct lecturer at SCU, CA, USA and principal research scientist at ASDRP, CA, USA and remaining authors, graduate students at SCU declares that research was conducted in absence any commercial or financial relationships that could be construed as a potential conflict of interest.

DATA AVAILABILITY STATEMENTS

Research data may be available upon written request.

AUTHOR CONTRIBUTION

Dr. Starostina lead original research, manuscript preparation and submission. The remaining authors contributed with data acquisition, data analysis, literature research and overview draft writing.

REFERENCES

1. Brooks I, et al. Analysis of hardness–tensile strength relationships for electroformed nanocrystalline materials. Mater Sci Eng A. 2008;491:412-419.
2. Walley SM. Historical origins of indentation hardness testing. Mater Sci Technol. 2012;28:1028-1044. [
3. Mobley RK. Predictive Maintenance Techniques. (2nd edn). Amsterdam; Elsevier, Netherlands, 2002.
4. Jia D, et al. 2020 International Pipeline Conference (Vol. 84461, P. V003T05A022). American Society of Mechanical Engineers. 2020.
5. Fujita M, et al. An evaluation of mechanical properties with the hardness of building steel structural members for reuse by NDT. Metals. 2016;10:247.
6. Selcuk S. Predictive maintenance, its implementation and latest trends. Manuf Eng. 2017;9:1670-1679.
7. Zonta T, et al. Predictive maintenance in the Industry 4.0: A systematic literature review. CAIE. 2020;150:106889.
8. Pamukchieva V, et al. Microhardness and elastic properties of bulk glasses and thin films of the Ge/sub x/-Sb/sub 40-x/-S/sub 60/ family. IEEE. 1996;2:373-376.
9. Rao BC, et al. Determination of tensile properties of lead-free solder joints using nanoindentation. IEEE. 2010;12:309-314.
10. Hossain A, et al. Factors affecting spherical nano-indentaton of thin film/substrate system. ASME. 2014;46590:V010T13A021.
11. EO Hall. The deformation and ageing of mild steel: III discussion of results. Proc Phys Soc Sect B. 1951;9:747-755.
12. NJ Petch. The cleavage strength of polycrystals. J Iron Steel Inst. 1953;1:25-28.

13. Cordero ZC, et al. Six decades of the hall–petch effect–A survey of grain-size strengthening studies on pure metals. Int Mater Rev. 2016;8:495512.
14. Askeland DR, et al. The Science and Engineering of Materials. (6th edn). Stamford; Cengage Learning, USA.2014.
15. Callister WD, et al. Materials Science and Engineering: An Introduction. (10th edn). Hoboken; Wiley, USA. 2018.
16. Kumar KS, et al. Mechanical behavior of nanocrystalline metals and alloys. Acta Mater. 2003;19:5743-5774.
17. Khodabakhshi F, et al. On the correlation between indentation hardness and tensile strength in friction stir processed materials. Mater Sci Eng A. 2020;789:139682.
18. Tabo D. The hardness and strength of metals. J. Inst. Metals. 1951;79:1-18.
19. Cahoon JR. An improved equation relating hardness to ultimate strength. MMTB. 1972;3:3040-3040.
20. Tabor D. Indentation hardness: Fifty years on a personal view. Phil Mag. 1996;74:1207-1212.
21. Broitman E. Indentation hardness measurements at macro-, micro- and nanoscale: A critical overview. tribol lett. 2017;65:23.
22. Pintaude G. Hardness as an indicator of material strength: A critical review. Crit Rev Solid State Mater Sci. 2022;48:1-19.
23. Khodabakhshi F, et al. Hardness–strength relationships in fine and ultra-fine grained metals processed through constrained groove pressing. Mater Sci Eng A. 2015;636:331-339.
24. Zhang P, et al. General relationship between strength and hardness. Mater Sci Eng A. 2011;529:62-73.
25. Yakubtsov IA, et al. Microstructure and mechanical properties of bainitic low carbon high strength plate steels. Mater Sci Eng A. 2008;480:109-116.
26. Knapp JA, et al. Finite-element modeling of nanoindentation. J Appl Phys. 1999;85:1460-1474.
27. Sawa T. Correlation between nanoindentation test result and vickers hardness. IMEKO. 2010;171-174.
28. Oliver WC, et al. An improved technique for determining hardness and elastic modulus using load and displacement sensing indentation experiments. J Mater Sci Res. 1992;7:1564-1583.
29. Taylor MD, et al. Correlations between nanoindentation hardness and macroscopic mechanical properties in DP980 steels. Mater Sci Eng A. 2014;597:431-439.
30. Geng D, et al. Toward the correlation of indentation hardness in micro- and nano-scale: Understanding of indentation edge behaviors in Fe–Cr alloys. J Mater Sci. 2022;57:13736-13755.
31. Shuman DJ, et al. Calculating the elastic modulus from nanoindentation and microindentation reload curves. Mater Charact. 2007;58:380-389.
32. Armstrong RW, et al. Elastic, plastic, cracking aspects of the hardness of materials. Int J Mod Phys B. 2013;27:1330004.
33. Xiaowu H, et al. Research on lamellar structure and micro-hardness of directionally solidified Sn-58 Bi eutectic alloy. China Foundry. 2012;9:360-365.
34. Shen L, et al. Elastic modulus, hardness and creep performance of SnBi alloys using nanoindentation. Mater Sci Eng A. 2012;558:253-258.
35. Hua F, et al. Eutectic Sn-Bi as an alternative to Pb-free solders. ECTC. 1998;48:277-283.
36. Torres A, et al. Effect of antimony additions on corrosion and mechanical properties of sn-bi eutectic lead-free solder alloy.MSA.2012;3:352-362.

37. Ribas M, et al. Development of low-temperature drop shock resistant solder alloys for handheld devices. IEEE. 2013;48-52.
38. Silva BL, et al. Complex eutectic growth and Bi precipitation in ternary Sn-Bi-Cu and Sn-Bi-Ag alloys. J Alloys Compd. 2017;691:600-605.
39. Silva BL, et al. Microstructural development and mechanical properties of a near-eutectic directionally solidified Sn–Bi solder alloy. Mater Charact. 2015;104:43-53.
40. Wang F, et al. Recent progress on the development of Sn–Bi based low-temperature Pb-free solders. J Mater Sci Mater Electron. 2019;30:3222-3243.
41. Wang F, et al. Interfacial reaction and mechanical properties of sn-bi solder joints. Materials (Basel). 2017;10:920.
42. Lee BJ, et al. Phase diagrams & computational thermodynamics. NIST. 1996;983-991.
43. Zhang K, et al. Mechanical properties and constitutive model of Sn-58Bi alloy. Mater Res Express. 2022;9:016505.
44. An Z, et al. Mechanically strengthened Graphene-Cu composite with reduced thermal expansion towards interconnect applications. MEMS NEMS.2019;5:20.
45. Subramanian KS, et al. Water contamination: Impact of tin-lead solder. Watre Res. 1995;29:1827-1836.
46. Almeida CM, et al. Assessing the replacement of lead in solders: Effects on resource use and human health. J Clean Prod. 2013;47:457-464.
47. Berkovich ES. Three-faceted diamond pyramid for micro-hardness testing. Ind Diamond Rev. 1951;11:129.
48. Khrushchov MM, et al. Methods of determining the hardness of very hard materials: The hardness of diamond. Ind Diamond Rev. 1951;11:42-49.
49. Bishop HE. Some electron backscattering measurements for solid targets, in Optique des Rayons X et Microanalyse. X-ray Optics Microanal. 1966;1:153-158.
50. Chadwick GA. Interlamellar spacing measurements in certain binary eutectic systems. OSTI GOV. 1962.
51. Goldstein, JI, et al. Scanning electron microscopy and x-ray microanalysis. Springer. 2017.
52. Castaing R, et al. X-ray optics and microanalysis. Hermann. 1966.
53. Voyiadjis GZ, et al. Review of nanoindentation size effect: Experiments and atomistic simulation. 2017;7:321.